46th AIAA/ASME/SAE/ASEE Joint Propulsion Conference & Exhibit
25 - 28 July 2010, Nashville, TN

AIAA 2010-7080

Quasi-Analytical Approximation of the Compressible Flow in a Planar Rocket Configuration

Michel Akiki* and Joseph Majdalani†
University of Tennessee Space Institute, Tullahoma, TN 37388

This work provides a semi-analytical formulation that oversees the details of the rotational, steady, inviscid, compressible motion in a solid rocket motor. By assuming a slender porous chamber, the method that we follow reduces the problem's mass, momentum, energy, ideal gas, and isentropic relations into a single integral equation that can be solved numerically. Furthermore, the dependence of the sidewall mass injection on the pressure inside the chamber is introduced by the use of Saint-Robert's power law. At first, the analysis overcomes some of the deficiencies encountered in previous work on the subject. Results are then presented and compared to two closed-form analytical solutions developed under one-dimensional and two-dimensional isentropic flow conditions by assuming either uniformly distributed mass flux or constant injection speed along the length of the propellant grain. In this work, agreement with the one-dimensional solution is demonstrated for the case with uniform mass flux at the wall. For a constant sidewall injection velocity, our formulation compares favorably with the two-dimensional asymptotic approximation obtained by Maicke and Majdalani (Maicke, B. A., and Majdalani, J., "On the Rotational Compressible Taylor Flow in Injection-Driven Porous Chambers," *Journal of Fluid Mechanics,* Vol. 603, No. 1, 2008, pp. 391-411). Moreover, a comparison with experimental data by Traineau, Hervat, and Kuentzmann (Traineau, J. C., Hervat, P., and Kuentzmann, P., "Cold-Flow Simulation of a Two-Dimensional Nozzleless Solid-Rocket Motor," AIAA Paper 86-1447, July 1986) helps to validate the present solution.

Nomenclature

a	=	chamber half-height
c_p	=	constant pressure specific heat
L_0	=	length of chamber
L_s	=	sonic length (critical distance)
M	=	Mach number
m	=	injection mass flux
P	=	nondimensional pressure
p	=	dimensional pressure
y	=	coordinate normal to the propellant surface
T	=	temperature
U_w	=	wall injection velocity
u	=	axial velocity
v	=	radial velocity
X	=	nondimensional axial coordinate
x	=	dimensional axial coordinate
ψ	=	streamfunction
χ	=	axial coordinate referenced to the sonic length, x / L_s

*Graduate Research Assistant, Mechanical, Aerospace and Biomedical Engineering Department. Member AIAA.
†H. H. Arnold Chair of Excellence in Advanced Propulsion, Mechanical, Aerospace and Biomedical Engineering Department. Senior member AIAA. Fellow ASME.

γ = ratio of specific heats
ρ = density
ξ = distance from the headwall to the tip of the streamline at the sidewall

Subscripts
c = choking conditions
w = wall conditions

I. Introduction

IN the fluid mechanics discipline, one can identify three main avenues for solving a problem, namely, analytical, computational and experimental. While experimental procedures can require substantial investments in time and resources, computational methods can prove to be no less time consuming and laborious. And though analytical techniques can be somewhat challenging to apply, they often lead to deeper physical insight that, otherwise, cannot be gained using either of the two more common methods of investigation. In short, all three approaches remain indispensable and fundamentally interdependent. With the remarkable progress achieved in computational platforms, numerical simulations have evolved to the point of granting us the ability to model complex systems, especially when implemented with a suitable set of governing equations and constitutive relations. Technically, however, the accuracy of new computational routines remains questionable until validated in a post-predictive framework, often based on laboratory measurements and limiting process analytical approximations. From this perspective, it may be safe to say that the physical understanding of fundamental mechanisms underlying fluid motion can substantially benefit from theoretical analyses, such as those developed here.

Rocket propulsion, a tool on which the world's communication structure is built, stands as a field in which many advances are yet to be made, theories to be developed, and phenomena to be explored. For example, among chemical propulsion systems, solid rocket motors are often idealized as porous chambers in which the effects of compressibility can be either retained or dismissed, depending on the gas injection speed and chamber length. In this regard, one of the most cited models remains, perhaps, Taylor's incompressible analytical representation,[1] which was introduced to the aerospace community by Culick in 1966.[2] Subsequent advances have enabled us to account for the presence of arbitrary headwall injection,[3,4] wall regression,[5,6] and variable chamber cross section.[7] In connection with the present study, compressible flow effects in simulated solid rocket motors have been investigated by Dunlap, Willoughby and Hermsen,[8] and then by Traineau, Hervat and Kuentzmann.[9] Both groups of investigators have conducted cold flow experiments in porous ducts in which characteristics of the spatially developing motion have been reported, including appreciable steepening beyond the incompressible Taylor-Culick base flow.[1,2] The flattening of the mean velocity profiles, which became more pronounced as the gases advanced downstream, has prompted additional numerical simulations by Beddini,[10] Baum, Levine and Lovine,[11] Liou and Lien,[12] and Apte and Yang.[13] Interest in quantifying the compressible Taylor-Culick motion and its hydrodynamic instability may also be seen in the works of Venugopal[14] and Wasistho, Balachandar and Moser.[15] These have also attempted to simulate the compressible mean flow motion in rocket chambers under nonreactive conditions.

In the present study, we focus our attention on two theoretical techniques that have been previously considered in the treatment of this problem. The first is a variant of the Prandtl-Glauert expansion,[16] which was first developed by Traineau, Hervat and Kuentzmann,[9] and later revisited by Balakrishnan, Liñan and Williams,[17] both in the context of inviscid, rotational, isentropic and compressible motion in wall injected ducts. The technique in question invokes scaling arguments to justify the dismissal of the y-momentum equation. This step is followed by the reduction of the remaining momentum, mass, energy, ideal gas and isentropic state relations to a single integral expression that can be solved numerically. The second technique denotes a variant of the Rayleigh-Janzen expansion. This technique was first employed by Majdalani[18] and then by Maicke and Majdalani[19] in the compressible treatment of both axisymmetric and planar chamber configurations. The attending procedure consists of expanding the governing equations in terms of a small perturbation parameter taken to be the square of the wall injection Mach number. The resulting analysis gives rise to two explicit solutions that describe the motion of two-dimensional compressible gases in porous chambers. At the outset, a self-similar, parameter-independent behavior is reported irrespective of the wall Mach number so long as the axial variable is rescaled by the critical distance from the headwall to the point at which sonic conditions are achieved. In this study, these models will be compared to one another and to a closed-form analytical solution representing, in the context of nozzleless rocket motors, a one-dimensional flow approximation due to Gany and Aharon.[20] The objective of this study is hence to reconstruct and

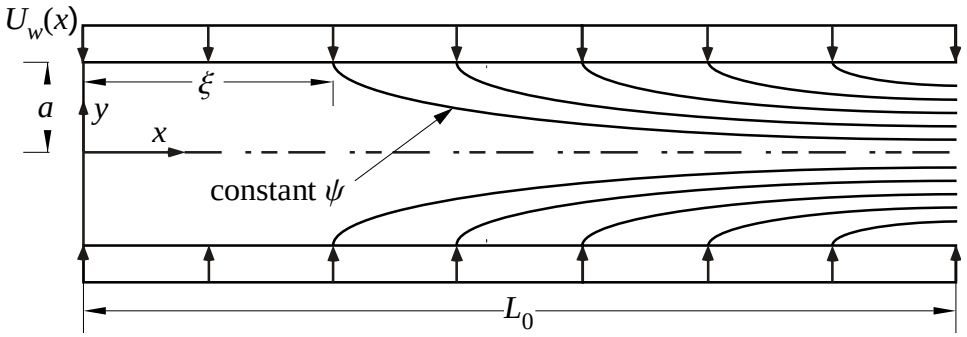

Figure 1. Schematic diagram of a slender porous chamber.

extend the integral formulation initiated by Traineau, Hervat and Kuentzmann,[9] such that a clear and verifiable pseudo-two-dimensional approximation may be deduced, specifically, one that can be compared to the one- and two-dimensional representations obtained using asymptotic tools.

II. Mathematical Model

A. Geometry

The domain under investigation extends horizontally from $x = 0$ to $x = L_0$, and vertically from the center axis to the wall, where the top and bottom plates may be viewed as symmetrical porous sidewalls across which flow is injected at a velocity $U_w(x)$. A schematic diagram of the planar problem is given in Fig. 1.

B. Formulation

A solid rocket motor can be modeled as a slender, elongated chamber with sidewall injection. Under the assumption of low chamber aspect ratio, $a / L_0 << 1$, the system's conservation equations may be conveniently reduced to the following set:

$$\frac{\partial(\rho u)}{\partial x} + \frac{\partial(\rho v)}{\partial y} = 0 \text{ (compressible continuity)} \tag{1}$$

$$\rho u \frac{\partial u}{\partial x} + \rho v \frac{\partial u}{\partial y} = -\frac{\partial p}{\partial x} \text{ (x–momentum)} \tag{2}$$

$$\frac{\partial p}{\partial y} = 0 \text{ (y–momentum)} \tag{3}$$

and

$$\rho u \frac{\partial}{\partial x}\left(c_p T + \frac{u^2}{2} \right) + \rho v \frac{\partial}{\partial y}\left(c_p T + \frac{u^2}{2} \right) = 0 \text{ (energy)} \tag{4}$$

Note that the chamber's low aspect ratio has resulted in the dismissal of the pressure variations in the y direction. Furthermore, the gas is assumed to be ideal with a constant c_p such that

$$p = \frac{\gamma - 1}{\gamma} c_p \rho T \text{ (ideal gas)} \tag{5}$$

For energy conservation, Eq. (4) may be rearranged into

$$\rho u c_p \frac{\partial T}{\partial x} + \rho v c_p \frac{\partial T}{\partial y} + u\left(\rho u \frac{\partial u}{\partial x} + \rho v \frac{\partial u}{\partial y} \right) = 0 \tag{6}$$

The term that appears between parentheses stems from the left-hand-side of the momentum equation. One can substitute Eqs. (2) and (5) into Eq. (6) to produce

$$\rho u\left(\frac{\partial T}{\partial x} - \frac{\gamma - 1}{\gamma} \frac{T}{p} \frac{\partial p}{\partial x} \right) + \rho v \frac{\partial T}{\partial y} = 0 \tag{7}$$

Then, inserting $\phi = T / p^{(\gamma-1)/\gamma}$ into Eq. (7), one obtains

$$\rho u\frac{\partial \phi}{\partial x}+\rho v\frac{\partial \phi}{\partial y}=0,\quad \rho \boldsymbol{u}\cdot\nabla\phi=0,\quad \text{or}\quad \rho\frac{\mathrm{D}\phi}{\mathrm{D}t}=0 \tag{8}$$

Since the material derivative vanishes in Eq. (8), it is clear that ϕ remains constant along a streamline.

C. Boundary Conditions

The physical requirements of the problem are used to define a consistent set of boundary conditions. These are:

$$\begin{cases} u(x,a)=0 & \text{(no slip at sidewall)} \\ u(0,y)=0 & \text{(no headwall injection)} \\ v(x,a)=-U_w(x) & \text{(normal sidewall injection)} \\ v(x,0)=0 & \text{(no cross-flow at the centerline)} \\ T(x,a)=T_w(x) & \text{(sidewall temperature)} \\ p(0)=p_0 & \text{(headwall pressure)} \end{cases} \tag{9}$$

We note that the injection velocity and the temperature at the sidewall are functions of x. In general, they may be permitted to vary with x, the longitudinal distance measured from the headwall.

D. Streamfunction Transformation

For planar motions, the streamfunction may be written as

$$\frac{\partial \psi}{\partial y}=\rho u,\quad \frac{\partial \psi}{\partial x}=-\rho v \tag{10}$$

Using a constant $\left(c_pT+u^2/2\right)$ along a streamline, one can put

$$T(x,\psi)+u^2(x,\psi)/(2c_p)=T_w(\psi) \tag{11}$$

As for ϕ, the isentropic pressure-temperature relation, its value along any streamline may be set equal to its value at the sidewall. This enables us to write

$$T(x,\psi)/\left[p(x)\right]^{(\gamma-1)/\gamma}=T_w(\psi)/\left[p_w(\psi)\right]^{(\gamma-1)/\gamma} \tag{12}$$

Given that all streamlines are initiated at the injecting walls, Eq. (10) may be evaluated at $y=a$. Then using the ideal gas expression for the density, subsequent integration in the x-direction yields

$$\psi=\frac{a\gamma}{(\gamma-1)c_p}\int_0^{\xi}\left[U_w(x)\,p(x)/T_w(x)\right]\mathrm{d}x \tag{13}$$

At this point, one may recognize that there exists a unique value of ψ associated with a given ξ, the distance from the headwall to the tip of a streamline taken at the sidewall. At the outset, the independent variables may be transformed from (x,ψ) to (x,ξ). When this pair is substituted into Eqs. (11) and (12), we get

$$T(x,\xi)+u^2(x,\xi)/(2c_p)=T_w(\xi) \tag{14}$$

$$T(x,\xi)/\left[p(x)\right]^{(\gamma-1)/\gamma}=T_w(\xi)/\left[p(\xi)\right]^{(\gamma-1)/\gamma} \tag{15}$$

Equation (13) can be readily substituted into Eq. (10) and integrated in the normal direction. This allows us to extract the coordinate y associated with a given position x and the streamline emanating from an arbitrary position ξ at the sidewall. We thus retrieve

$$y=\int_0^{\xi}\left[\frac{T(x,\xi')}{p(x)u(x,\xi')}\right]\left[\frac{U_w(\xi')\,p(\xi')}{T_w(\xi')}\right]\mathrm{d}\xi' \tag{16}$$

To express y in terms of the pressure only, Eqs. (14) and (15) may be straightforwardly substituted for the velocity and temperature. This operation yields

$$y=\int_0^{\xi}\left[\frac{p(\xi')}{p(x)}\right]^{1/\gamma}\left[1-\left[\frac{p(x)}{p(\xi')}\right]^{(\gamma-1)/\gamma}\right]^{-1/2}\frac{U_w(\xi')}{\sqrt{2c_pT_w(\xi')}}\mathrm{d}\xi' \tag{17}$$

Finally, recalling that $y=a$ at $\xi=x$, Eq. (17) may be recast in the form

$$a = \int_0^x \left[\frac{p(\xi)}{p(x)}\right]^{1/\gamma} \left\{1 - \left[\frac{p(x)}{p(\xi)}\right]^{(\gamma-1)/\gamma}\right\}^{-1/2} \frac{U_w(\xi)}{\sqrt{2c_p T_w(\xi)}} \mathrm{d}\xi \tag{18}$$

E. Integral Formulation with No Pressure Dependence

To simplify the analysis, three dimensionless variables $P(X)$, X and Ξ may be introduced. These are defined by

$$P(X) = \frac{p(x)}{p_0} \tag{19}$$

$$X = \sqrt{\frac{\gamma}{\gamma-1}} \frac{1}{a} \int_0^x \frac{U_w(x')}{\sqrt{2c_p T_w(x')}} \mathrm{d}x' = \sqrt{\frac{\gamma}{2}} \frac{1}{a} \int_0^x M_w(x') \mathrm{d}x' \tag{20}$$

$$\Xi = \sqrt{\frac{\gamma}{\gamma-1}} \frac{1}{a} \int_0^\xi \frac{U_w(x')}{\sqrt{2c_p T_w(x')}} \mathrm{d}x' = \sqrt{\frac{\gamma}{2}} \frac{1}{a} \int_0^\xi M_w(x') \mathrm{d}x' \tag{21}$$

The above expressions may be inserted into Eqs. (17) and (18) to obtain

$$\frac{y}{a} = \sqrt{\frac{\gamma-1}{\gamma}} \int_0^\Xi \left[\frac{P(\Xi')}{P(X)}\right]^{1/\gamma} \left\{1 - \left[\frac{P(X)}{P(\Xi')}\right]^{(\gamma-1)/\gamma}\right\}^{-1/2} \mathrm{d}\Xi' \tag{22}$$

$$\sqrt{\frac{\gamma}{\gamma-1}} = \int_0^X \left[\frac{P(\Xi)}{P(X)}\right]^{1/\gamma} \left\{1 - \left[\frac{P(X)}{P(\Xi)}\right]^{(\gamma-1)/\gamma}\right\}^{-1/2} \mathrm{d}\Xi \tag{23}$$

F. Integral Formulation with Pressure Dependence

One can link the mass flux at the wall, $m_w(\xi)$, to the local pressure, $p(\xi)$, by assuming a dependence on the burning-rate that follows Saint-Robert's law with constant K and n. This can be achieved by setting

$$m_w = \rho_w U_w = K p^n \tag{24}$$

Substituting the density obtained from the ideal gas law, the accompanying wall injection velocity may be expressed as

$$U_w = \frac{\gamma-1}{\gamma} c_p \frac{T_w(\xi)}{p(\xi)} m_w(\xi) \tag{25}$$

Note that for $n = 0$, the wall mass flux remains constant along the length of the grain, whereas for $n = 1$, the sidewall boundary experiences a uniform injection velocity profile. The resulting U_w may be introduced into Eq. (18) to retrieve the dimensionless forms of $P(X)$, X and Ξ. These are

$$P(X) = \frac{p(x)}{p_0} \tag{26}$$

$$X = \sqrt{\frac{\gamma-1}{\gamma}} \frac{K p_0^{n-1}}{2a} \int_0^x \sqrt{2c_p T_w(x')} \mathrm{d}x' \tag{27}$$

$$\Xi = \sqrt{\frac{\gamma-1}{\gamma}} \frac{K p_0^{n-1}}{2a} \int_0^\xi \sqrt{2c_p T_w(x')} \mathrm{d}x' \tag{28}$$

At length, Eqs. (17) and (18) become

$$\frac{y}{a} = \sqrt{\frac{\gamma-1}{\gamma}} \int_0^\Xi \left[P(\Xi')\right]^{n-1} \left[\frac{P(\Xi')}{P(X)}\right]^{1/\gamma} \left\{1 - \left[\frac{P(X)}{P(\Xi')}\right]^{(\gamma-1)/\gamma}\right\}^{-1/2} \mathrm{d}\Xi' \tag{29}$$

and

$$\sqrt{\frac{\gamma}{\gamma-1}}=\int_0^X\left[P(\Xi)\right]^{n-1}\left[\frac{P(\Xi)}{P(X)}\right]^{1/\gamma}\left\{1-\left[\frac{P(X)}{P(\Xi)}\right]^{(\gamma-1)/\gamma}\right\}^{-1/2}\mathrm{d}\Xi \tag{30}$$

To solve this problem, one starts by integrating Eq. (30) to the extent of determining the pressure as a function of x. By numerically evaluating Eq. (29), the radial coordinate may be resolved in terms of x and ξ. With the pressure distribution at hand, the temperature may be subsequently deduced from the isentropic ratio given by Eq. (15). The velocity may be similarly extracted from the total temperature relation given by Eq. (14).

To calculate the Mach number, the compressible flow relation $M=u/\sqrt{(\gamma-1)c_pT}$ may be employed. In fact, the substitution of Eq. (14) into the Mach number relation gives

$$M=\sqrt{\left(\frac{2}{\gamma-1}\right)\left[\frac{T_w(\xi)}{T(x,\xi)}-1\right]}=\sqrt{\left(\frac{2}{\gamma-1}\right)\left[\left(\frac{P(\Xi)}{P(X)}\right)^{(\gamma-1)/\gamma}-1\right]} \tag{31}$$

where the right-hand-side expression takes advantage of the isentropic identity realized through Eq. (15).

G. Numerical Procedure

For the numerical integration of Eq. (30), the independent variable is chosen to be P such that X may be calculated in increments of ΔP. The starting point of the iterative process may be anchored at the headwall where $X=0$ and $P=1$. The limiting condition occurs when $\mathrm{d}P/\mathrm{d}X\to\infty$, thus signaling the onset of choked flow. At this juncture, transforming the independent variable in Eq. (30) leads to

$$\sqrt{\frac{\gamma-1}{\gamma}}\int_P^1(P')^{n-1}\left(\frac{P'}{P}\right)^{1/\gamma}\left[1-\left(\frac{P}{P'}\right)^{(\gamma-1)/\gamma}\right]^{-1/2}\left[-\frac{\mathrm{d}X(P')}{\mathrm{d}P'}\right]\mathrm{d}P'=\int_P^1 f(P')\,\mathrm{d}P'=1 \tag{32}$$

To overcome endpoint singularities, the above integral may be split into three parts. This decomposition is intended to segregate the leftmost and rightmost cell intervals as labeled below:

$$\int_P^1 f(P')\,\mathrm{d}P'=\underbrace{\int_{P_i}^{P_{i-1}} f(P')\,\mathrm{d}P'}_{\boxed{1}}+\underbrace{\int_{P_{i-1}}^{1-\Delta P} f(P')\,\mathrm{d}P'}_{\boxed{2}}+\underbrace{\int_{1-\Delta P}^{1} f(P')\,\mathrm{d}P'}_{\boxed{3}}=1 \tag{33}$$

In the region near $P=P_i$, the first integrand may be approximated by

$$\int_{P_i}^{P_{i-1}} f(P')\,\mathrm{d}P'\approx\int_{P_i}^{P_{i-1}}(P')^{n-1}\left(\frac{P'-P_i}{P'}\right)^{-1/2}\left(-\frac{\mathrm{d}X}{\mathrm{d}P'}\right)_i\mathrm{d}P' \tag{34}$$

This expression may be evaluated differently based on the value of n. We find

$n=0$:
$$\int_{P_i}^{P_{i-1}} f(P')\,\mathrm{d}P'\approx 2\,ln\left(\frac{\sqrt{P_i+\Delta P}+\sqrt{\Delta P}}{\sqrt{P_i}}\right)\frac{(X_i-X_{i-1})}{\Delta P} \tag{35}$$

$n=1$:
$$\int_{P_i}^{P_{i-1}} f(P')\,\mathrm{d}P'\approx\left[P_i\,ln\left(\frac{\sqrt{P_i+\Delta P}+\sqrt{\Delta P}}{\sqrt{P_i}}\right)+\sqrt{\Delta P}\sqrt{\Delta P+P_i}\right]\frac{(X_i-X_{i-1})}{\Delta P} \tag{36}$$

To compute the second integral, the trapezoidal rule may be used viz.

$$\int_{P_{i-1}}^{1-\Delta P} f(P')\,\mathrm{d}P'\approx\Delta P\left(\frac{f_1+f_{i-1}}{2}+\sum_{k=2}^{i-2}f_k\right) \tag{37}$$

where

$$f_k=\sqrt{\frac{\gamma-1}{\gamma}}\left[P_k\right]^{n-1}\left[\frac{P_k}{P_i}\right]^{1/\gamma}\left[1-\left(\frac{P_i}{P_k}\right)^{(\gamma-1)/\gamma}\right]^{-1/2}\left(-\frac{\mathrm{d}X}{\mathrm{d}P}\right)_k \tag{38}$$

In the third integral, X remains small. Consequently, $P(X)$ may be suitably expanded using a polynomial of the form

$$P(X)=1-\alpha X^2+\ldots \tag{39}$$

Inserting Eq. (39) into the integral and assuming $\alpha\Xi^2<<1$, we have

$$\int_{1-\Delta P}^{1} f(P')\,\mathrm{d}P' \approx \sqrt{\frac{\gamma-1}{\gamma}}\left(P_i\right)^{-1/\gamma}\left[1-\left(P_i\right)^{(\gamma-1)/\gamma}\right]^{-1/2}\sqrt{\frac{\Delta P}{\alpha}} \tag{40}$$

To evaluate Eq. (40), it is necessary to know α. This is achieved by substituting Eq. (39) into Eq. (30) and extracting

$$\frac{1}{\sqrt{\alpha}}\int_0^X \frac{1}{\sqrt{X^2-\Xi^2}}\,\mathrm{d}\Xi = 1 \tag{41}$$

This enables us to deduce that $\alpha = \frac{1}{4}\pi^2$.

To sketch the solution procedure, we make use of the linearity of Eq. (32) in X_i. Therefore, starting with $X = 0$ at $P = 1$, one may solve for X_i at every step until choking conditions are reached. Choking occurs at a point where P approaches its limiting value at an infinitely steep slope where the average Mach number reaches unity. With the pressure distribution being fully determined, it may be employed in Eq. (29) and integrated numerically. This returns the value of y that is needed for the complete description of the streamlines. Equations (14) and (15) may then be recalled to extract the temperature and velocity.

III. Results and Discussion

When considering the flow motion in planar porous chambers, one may consider Maicke and Majdalani[19] who were the first to construct a closed-form solution for the two-dimensional problem. Using techniques similar to the ones applied to the cylindrical case,[18] they introduced compact expressions that describe the mean flowfield in a porous duct extending from the headwall to the point where fully-choked conditions are reached. For the reader's convenience, the Maicke-Majdalani model may be summarized by enumerating its key components. These are:

$$\psi = x\sin\left(\tfrac{1}{2}\pi y\right) + M_w^2\left[-\tfrac{1}{48}x\sin\left(\tfrac{1}{2}\pi y\right)\left\{\pi^2x^2\left[3+\cos\left(\pi y\right)\right]+3\left[7-\cos\left(\pi y\right)\right]\right\}\right] \tag{42}$$

$$P_c = 1 - M_w^2\gamma\left(\tfrac{1}{8}\pi^2x^2\right) - M_w^4\left(\tfrac{1}{384}\gamma\pi^4x^4 - \tfrac{3}{32}\gamma\pi^2x^2 + \tfrac{1}{8}\gamma\right) \tag{43}$$

$$T_c = 1 + M_w^2\,\tfrac{1}{2}(1-\gamma)\left[\tfrac{1}{4}\pi^2x^2\right] + M_w^4\left\{\tfrac{1}{192}(1-\gamma)\left[2\pi^4x^4 - 18\pi^2x^2 + 24\right]\right\} \tag{44}$$

$$L_s = \frac{1}{\pi M_w}\sqrt{\frac{\phi_a^{2/3} - 8\phi_a^{1/3}(\gamma+1) + 32\left(2\gamma^2+\gamma-1\right)}{\phi^{1/3}}} \tag{45}$$

where

$$\phi_a = -128\left[\left(4\gamma^3+3\gamma^2-6\gamma-14\right)\right] + 3\sqrt{-\left(3\gamma^4+14\gamma^3+6\gamma^2-18\gamma-22\right)} \tag{46}$$

Another analytical solution found in the literature corresponds to a historical one-dimensional model revisited by Gany and Aharon.[20] The relation in question applies to an isentropic flow with the underlying assumption that the instantaneous burning rate remains uniform along the grain, thus leading to a constant mass flux at the simulated propellant surface. The ensuing one-dimensional Mach number, pressure, and temperature may be expressed as

$$M_{1\mathrm{D}} = \sqrt{\frac{1-\sqrt{1-\chi^2}}{1+\gamma\sqrt{1-\chi^2}}} \tag{47}$$

$$P_{1\mathrm{D}} = (1+\gamma)^{-1}\left(1+\gamma\sqrt{1-\chi^2}\right) \tag{48}$$

$$T_{1\mathrm{D}} = (1+\gamma)^{1/\gamma-1}\left(1+\gamma\sqrt{1-\chi^2}\right)^{1-1/\gamma} \tag{49}$$

Concerning the calculation of the critical distance, our computation of L_s leads to a sonic length that matches, within 7%, the value predicted by Eq. (45). On this note, it should be borne in mind that, according to Majdalani,[18] the critical length denotes, in the classic sense, the distance from the headwall to the point at which the centerline velocity first reaches the speed of sound. At that station, the area-averaged Mach number would not have reached unity yet. However, in order to reconcile with one-dimensional predictions (in which values are essentially area-averaged at a given axial station) a new definition is warranted, namely that of an area-averaged critical length, $\bar{L}_s$. Accordingly, a cross-section will be fully choked when its local average Mach number reaches unity. This condition always occurs downstream of the classical sonic point, at $\bar{L}_s > L_s$.

After solving Eq. (32) in decrements of ΔP, the pressure may be reproduced as a function of the axial distance. For constant mass flux ($n = 0$), results for the central pressure and temperature are illustrated in Figs. 2a and 2b, respectively. The improved agreement between the one-dimensional expression and our model is justified by virtue of their similar boundary conditions, including the specification of uniform mass flux at the sidewall. Also shown on the figure are experimental data points acquired by Traineau *et al.*[9] These researchers have considered the planar chamber with uniformly distributed mass addition. At first glance, it may be surprising to note the improved agreement that stands between experimental measurements and the one-dimensional model. This may be attributed to the dismissal of viscous effects and other sources of damping and irreversibilities that reduce the conversion of thermal energy to kinetic motion, thus building up the pressure in the chamber. Unlike the two dimensional model in

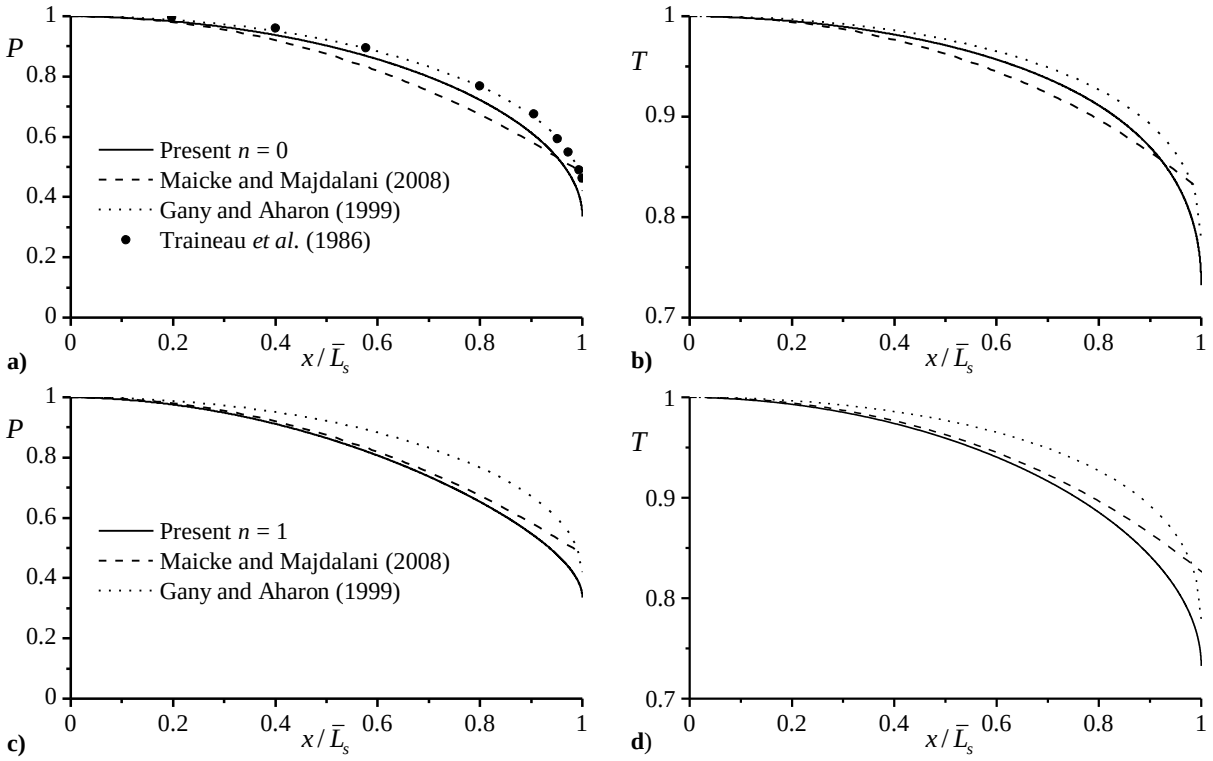

Figure 2. Comparison between the present semi-analytical formulation and both 1D and 2D solutions by Gany and Aharon[20] and Maicke and Majdalani.[19] Also featured are experimental results due to Traineau *et al.*[9] Results are shown for γ=1.4 and M_w = 0.05.

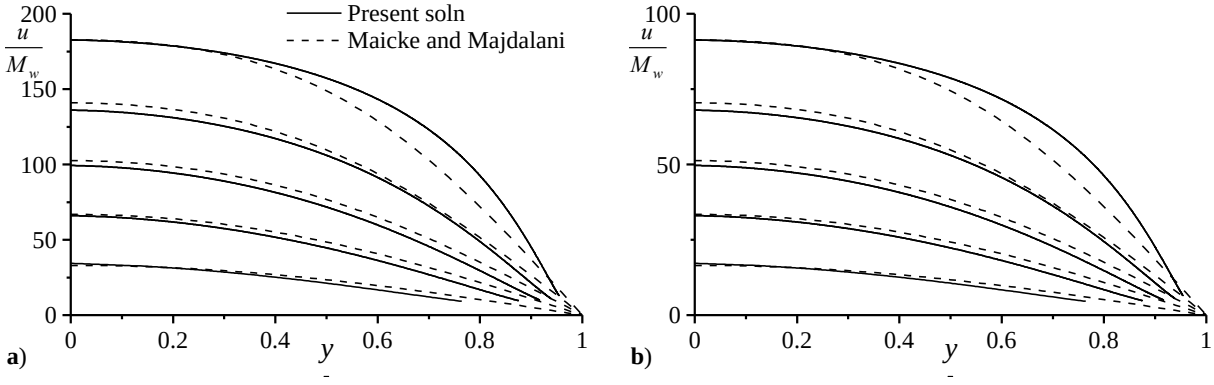

Figure 3. Spatial evolution of the axial velocity for a) M_w = 0.005 and b) M_w = 0.01 at x / L_s = 0.2, 0.4, 0.6, 0.8, and 1. Results are compared to the 2D axisymmetric solution by Maicke and Majdalani.[19] Here γ = 1.4.

which friction leads to additional increments in irreversibilities, the one-dimensional model appears to be less susceptible to these discrepancies due to its mass injection being fundamentally axial.

Figures 2c-d display the results for the $n=1$ case. The present solution seems to display excellent agreement with the analytical relations by Maicke and Majdalani.[19] The slight disparity around the choking region may be connected to the linear approximations used in the numerical procedure. These approximations may deteriorate as the critical distance is approached.

The evolution of the axial velocity profile throughout the chamber is illustrated in Fig. 3 along with the 2D analytical solution by Maicke and Majdalani.[19] As expected, the results demonstrate similar trends as the flow travels downstream. Compared to the incompressible Taylor solution, the compressible profiles display a steepening effect that is accompanied by higher velocity gradients near the wall. This steepening is also reflected in the experimental data collected by Traineau *et al*.[9]

Shifting attention to Fig 4, a favorable agreement may be reported between the present solution and the experimental data, specifically at locations where the flow remains nearly incompressible, (i.e. before the flow reaches 40% of the chamber). Advancing further downstream, steepening occurs and appears to be more pronounced in the experimental data. The disparity is justified by the dismissal of viscous and turbulence effects. These become more prominent as the flow approaches the sonic point.

Based on the numerical integration of Eq. (29), characteristic streamlines are extracted and displayed in Fig. 5. This step is carried out by first specifying a value of ξ, and then integrating at discrete locations of x. The procedure enables us to collect the family of coordinates at a fixed value of ξ, thus leading to an assortment of points that retrace a streamline. Figure 5 also shows Taylor's incompressible solution. The comparison reveals a faster turning of the flow that may be attributed to compressibility effects. Due to the strong similarity with respect to x/L_s, the ensuing graphs for any M_w become nearly identical when the axial length is rescaled, as shown in Fig 5b.

Using Eq. (31), one can calculate the Mach number over the entire chamber. Given that the variables are expressed in terms of the axial location and the streamline tip distance ξ, a transformation is required to revert back to the Cartesian coordinate system. The contour plot of the local Mach numbers is presented in Fig. 6 side-by-side

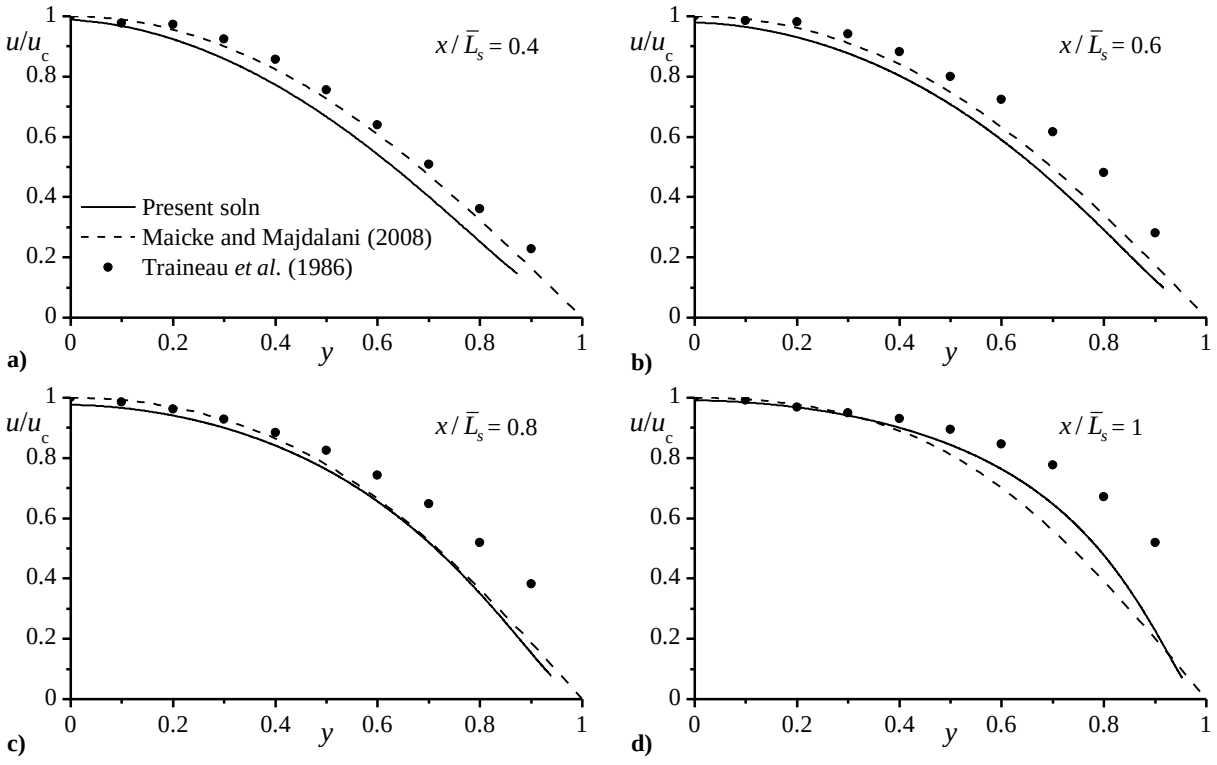

Figure 4. Axial velocity profiles obtained using the present formulation, the analytical solution by Maicke and Majdalani,[19] and experimental data taken from Traineau *et al*.[9]

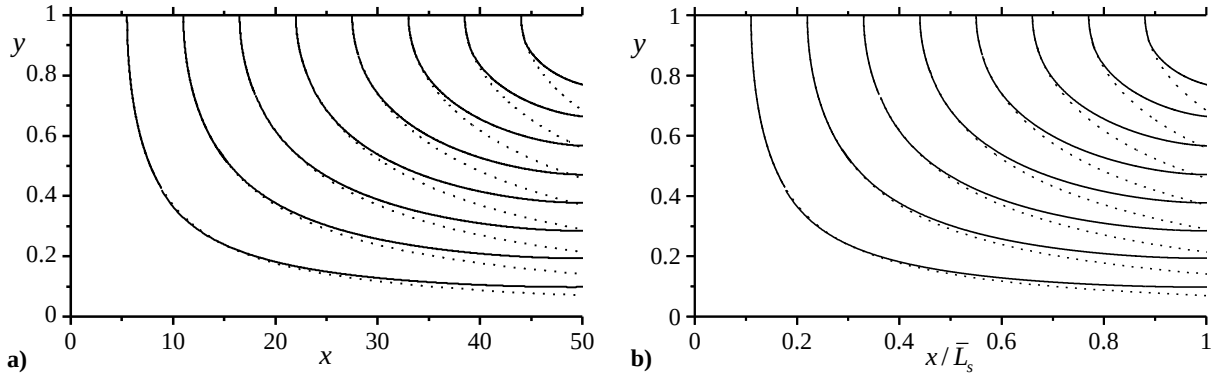

Figure 5. Numerical streamlines for M_w = 0.01, in solid lines, compared to the incompressible solution by Taylor,[1] in dotted lines. In b) the axial coordinate is rescaled by the critical length, thus leading to nearly perfect self-similarity.

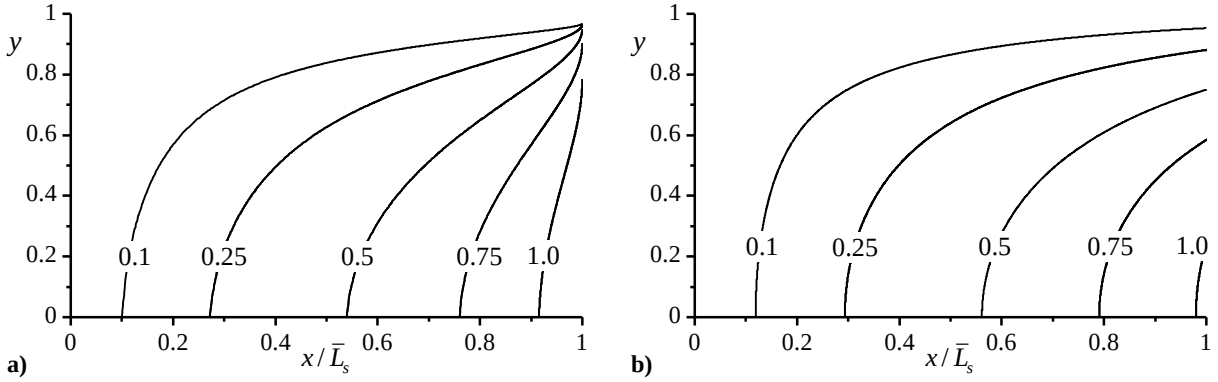

Figure 6. Local Mach number contours according to a) numerical integration and b) analytical solution by Maicke and Majdalani.[19]

with the two-dimensional analytical predictions for comparison. The models appear to be in fairly good agreement over the entire chamber, with dissimilarity around the choking region. Note that the flow hits $M=1$ at a curved line rather than a point. For that reason, we delineate choking to occur when the area-averaged Mach number reaches unity. Figure 6, being plotted versus $\chi = x/\bar{L}_s$, will remain the same if plotted for different values of wall Mach number. This is due to the geometric self-similarity with respect to χ.

IV. Conclusions

In this study, an integral formulation for compressible gas motion in a porous chamber is reconstructed and compared to one- and two-dimensional analytical approximations obtained under isentropic flow conditions. Unsurprisingly, the level of agreement is found to be commensurate with the sidewall boundary conditions associated with each of these models. In all cases, the main discrepancies occur near the sonic point and may be attributed to the various forms of approximations and linearization befalling the integral approach. The present investigation helps to confirm the theory introduced previously by Majdalani,[18] namely, the self-similarity with respect to the critical length. The study also confirms the steepening of velocity profiles and increased gradients at the sidewall due to compressibility. The technique presented here offers a key advantage in its ability to accommodate any sidewall injection or temperature profile, which could be later used to better mimic the propellant burning processes. On the other hand, the approach requires piecewise numerical integrations, sequential inversions, and backward transformations to retrieve the original variables of interest. This procedure may render the technique laborious compared to the simplicity with which the fully analytical models may be implemented and resolved.

Nonetheless, it remains more general and, once programmed, may entertain a variety of injection patterns that may be prescribed by the problem under investigation.

Acknowledgments

This project was funded by the National Science Foundation through Grant No. CMMI-0928762, Dr Eduardo A. Misawa, Program Director.

References

[1]Taylor, G. I., "Fluid Flow in Regions Bounded by Porous Surfaces," *Proceedings of the Royal Society of London, Series A,* Vol. 234, No. 1199, 1956, pp. 456-475. doi: 10.1098/rspa.1956.0050

[2]Culick, F. E. C., "Rotational Axisymmetric Mean Flow and Damping of Acoustic Waves in a Solid Propellant Rocket," *AIAA Journal,* Vol. 4, No. 8, 1966, pp. 1462-1464. doi: 10.2514/3.3709

[3]Barber, T. A., Maicke, B. A., and Majdalani, J., "Current State of High Speed Propulsion: Gaps, Obstacles, and Technological Challenges in Hypersonic Applications," AIAA Paper 2009-5118, August 2009.

[4]Majdalani, J., and Saad, T., "The Taylor-Culick Profile with Arbitrary Headwall Injection," *Physics of Fluids,* Vol. 19, No. 9, 2007, pp. 093601-10. doi: 10.1063/1.2746003

[5]Zhou, C., and Majdalani, J., "Improved Mean Flow Solution for Slab Rocket Motors with Regressing Walls," *Journal of Propulsion and Power,* Vol. 18, No. 3, 2002, pp. 703-711. doi: 10.2514/2.5987

[6]Majdalani, J., Vyas, A. B., and Flandro, G. A., "Higher Mean-Flow Approximation for a Solid Rocket Motor with Radially Regressing Walls," *AIAA Journal,* Vol. 40, No. 9, 2002, pp. 1780-1788. doi: 10.2514/1.40061

[7]Kurdyumov, V. N., "Steady Flows in the Slender, Noncircular, Combustion Chambers of Solid Propellants Rockets," *AIAA Journal,* Vol. 44, No. 12, 2006, pp. 2979-2986. doi: 10.2514/1.21125

[8]Dunlap, R., Willoughby, P. G., and Hermsen, R. W., "Flowfield in the Combustion Chamber of a Solid Propellant Rocket Motor," *AIAA Journal,* Vol. 12, No. 10, 1974, pp. 1440-1445. doi: 10.2514/3.49513

[9]Traineau, J. C., Hervat, P., and Kuentzmann, P., "Cold-Flow Simulation of a Two-Dimensional Nozzleless Solid-Rocket Motor," AIAA Paper 86-1447, July 1986.

[10]Beddini, R. A., "Injection-Induced Flows in Porous-Walled Ducts," *AIAA Journal,* Vol. 24, No. 11, 1986, pp. 1766-1773. doi: 10.2514/3.9522

[11]Baum, J. D., Levine, J. N., and Lovine, R. L., "Pulsed Instabilities in Rocket Motors: A Comparison between Predictions and Experiments," *Journal of Propulsion and Power,* Vol. 4, No. 4, 1988, pp. 308-316. doi: 10.2514/3.23068

[12]Liou, T.-M., and Lien, W.-Y., "Numerical Simulations of Injection-Driven Flows in a Two-Dimensional Nozzleless Solid-Rocket Motor," *Journal of Propulsion and Power,* Vol. 11, No. 4, 1995, pp. 600-606. doi: 10.2514/3.23886

[13]Apte, S., and Yang, V., "Effects of Acoustic Oscillations on Turbulent Flowfield in a Porous Chamber with Surface Transpiration," AIAA Paper 98-3219, July 1998.

[14]Venugopal, P., "Direct Numerical Simulation of Turbulence in a Model Solid Rocket Motor," Ph.D. Dissertation, University of Illinois at Urbana-Champaign, 2003.

[15]Wasistho, B., Balachandar, S., and Moser, R. D., "Compressible Wall-Injection Flows in Laminar, Transitional, and Turbulent Regimes: Numerical Prediction," *Journal of Spacecraft and Rockets,* Vol. 41, No. 6, 2004, pp. 915-924. doi: 10.2514/1.2019

[16]Zhiping, Z., Yongjie, N., and Qinggang, L., "Pressure Drop in Cyclone Separator at High Pressure," *Journal of Thermal Science,* Vol. 17, No. 3, 2008, pp. 275-280. doi: 10.1007/s11630-008-0275-7

[17]Balakrishnan, G., Liñan, A., and Williams, F. A., "Compressible Effects in Thin Channels with Injection," *AIAA Journal,* Vol. 29, No. 12, 1991, pp. 2149-2154. doi: 10.2514/3.10852

[18]Majdalani, J., "On Steady Rotational High Speed Flows: The Compressible Taylor-Culick Profile," *Proceedings of the Royal Society of London, Series A,* Vol. 463, No. 2077, 2007, pp. 131-162. doi: 10.1098/rspa.2006.1755

[19]Maicke, B. A., and Majdalani, J., "On the Rotational Compressible Taylor Flow in Injection-Driven Porous Chambers," *Journal of Fluid Mechanics,* Vol. 603, No. 1, 2008, pp. 391-411. doi: 10.1017/S0022112008001122

[20]Gany, A., and Aharon, I., "Internal Ballistics Considerations of Nozzleless Rocket Motors," *Journal of Propulsion and Power,* Vol. 15, No. 6, 1999, pp. 866-873. doi: 10.2514/2.5509